Nano Energy 67 (2020) 104217

Contents lists available at ScienceDirect

Nano Energy

journal homepage: http://www.elsevier.com/locate/nanoen

Full paper

Three-dimensional macroporous photonic crystal enhanced photon collection for quantum dot-based luminescent solar concentrator

Junyu Wang [a], Yucheng Yuan [a], Hua Zhu [a], Tong Cai [a], Yin Fang [b], Ou Chen [a,*]

[a] Department of Chemistry, Brown University, Providence, RI, 02912, United States
[b] Department of Chemical Engineering, University of Florida, Gainesville, FL, 32611, United States

ARTICLE INFO

Keywords:
Luminescent solar concentrator
Quantum dots
Photonic crystal
Escape cone loss
Solar energy

ABSTRACT

A luminescent solar concentrator (LSC) is a photon managing device that can harvest, direct and concentrate solar light to small areas, enabling subsequent coupling to photovoltaic devices (PVs) for enhanced solar energy conversion. However, the intrinsic photon loss through the so-called escape cone of the LSCs significantly limits their light harvesting and concentrating performance. In this work, we introduce a facile and low-cost approach for the fabrication of a three-dimensional (3D) macroporous photonic crystal (PC) filter as an efficient photon reflector, which can be coated onto quantum dot (QD) based LSC devices. We demonstrate that by controlling the PC reflection band to match the emission profile of the QD emitters, the light trapping efficiency of the PC coated LSC (PC-LSC) can be significantly improved from 73.3% to 95.1% as compared to the conventional PC-free LSC due to the reduced escape cone photon loss. In addition, we have developed a simulation model that considers the PC reflector effect. Both experimental and simulation results show that the enhancement in LSC device performance induced by the PC reflector increases with increasing dimension. In fact, simulation data predicts a maximum of 13.3-fold enhancement in external quantum efficiency (EQE) and concentration factor (C factor) of the PC-LSC under more ideal conditions. Moreover, the simulation result offers insight into the relationship between photon output efficiencies and the geometric design of the PC-LSC. Our study sheds light on future design and fabrication of LSC devices with enhanced photon collection and concentrating efficiencies through novel and wavelength-selective photon reflectors.

1. Background

Moving global energy consumption away from fossil fuels requires innovative, clean and cost-effective renewable energy technologies [1–4]. In this concern, solar power is the most abundant of all sustainable sources on our planet and harvesting solar energy utilizing photovoltaics (PVs) hold the highest potential capacity (~80 TW) among all renewable energy sources [5–12]. To this end, luminescent solar concentrators (LSCs) are innovative, cost-effective and large-area light collecting and concentrating devices that can be coupled to PVs for solar energy harvesting and conversion [13–17]. Depending on the utilized fluorophores, the LSCs can focus the broad range of wavelengths from sunlight into a confined wavelength range, then direct them to a smaller region of the device (light concentrating effect) for PV utilization [13,18]. Although the original idea for LSCs was initiated in the 1970s, significant developments have been recently demonstrated due to the advances of various high-quality emitters, especially semiconductor quantum dots (QDs) [17–29]. As a result of the geometric design and high refractive index of matrix materials utilized (*e.g.*, glass, polymer), the emitted photons can be largely trapped inside of the LSC through total internal reflection (TIR) as defined by Snell's law followed by further propagation to the edges of the LSC device [30–33]. In this light concentrating process, the energy output efficiency of LSCs is mainly limited by three major events: (1) The reabsorption process caused by partial overlap between absorption and emission spectra of the applied fluorophores; (2) energy loss through non-radiative decay channels due to the sub-unity photoluminescence quantum yield (PL QY) of the fluorophores; (3) photon loss through the escape cone of LSC devices. While the first two events can be greatly regulated by improving the absorption and emission qualities of the applied emitters [19–24,34,35], the escape cone photon loss has been recognized as an intrinsic limitation of LSCs [30–46]. Even for an ideal emitter with zero reabsorption behavior and unity PL QY, the escape cone photon loss of the LSC is still inevitable and invariant. Recent efforts in reducing this escape cone

* Corresponding author.
E-mail address: ouchen@brown.edu (O. Chen).

https://doi.org/10.1016/j.nanoen.2019.104217
Received 14 June 2019; Received in revised form 11 October 2019; Accepted 20 October 2019
Available online 5 November 2019
2211-2855/© 2019 Elsevier Ltd. All rights reserved.

photon loss include coating the LSC with organic cholesteric mirrors [37–39], two-dimensional (2D) photonic crystal (PC) distributed Bragg reflectors [28,33,36,40], silver and aluminum metal films [36,43], and rugate filters [44–46]. However, most of these reported Bragg filters possess non-selective broad reflection bands, and/or sophisticated fabrication processes not ideal for large-scale production, thus limiting their potentials in practical applications [47].

Herein, we introduce a 3D macroporous-structured PC coated QD-based LSC (PC-LSC) device as an alternative means to effectively reduce escape cone photon loss. We demonstrate that the stopband of PC layer can be programmed to serve as a highly selective wavelength reflector in order to perfectly match the emission profile of the applied emitters (*e.g.,* QDs). After PC coating on both the top and bottom of the LSC surfaces, light trapping efficiency of the PC-LSC can be dramatically increased by ~30% as compared to the conventional LSC without PC coating (PC-free LSC). Both experimental and simulation results reveal that this enhanced photon trapping capability leads to significant improvements for both the external quantum efficiency (EQE) and the concentration factor (C factor) of the resulting PC-LSC devices. Both EQE and C factor can be nearly doubled by the PC coating for large-area LSC devices under sunlight illumination, demonstrating their potentials for practical integration into solar energy conversion systems with enhanced energy harvesting capabilities.

2. Results and discussion

2.1. Working principle of PC-LSC devices

The escape cone photon loss is associated with an internal light beam angle that is smaller than the critical angle of LSC surface (shown in Fig. 1a, right). According to the LSC's refractive index (n), the trapping efficiency (η_{trap}) is defined as [30].

$$\eta_{trap} = \sqrt{1 - n^{-2}} = cos\theta_{esc} \quad (1)$$

where, θ_{esc} is the escape cone angle, which is defined by Snell's law as $\theta_{esc} = \arcsin\left(\frac{1}{n}\right)$. For a typical polymer matrix with *e.g.* $n = 1.5$, the η_{trap} is ~74.5% and θ_{esc} is 41.8°. This means ~25.5% of the emitted photons inside an LSC will be lost to the top/bottom surfaces through the escape cone, dramatically diminishing the light harvesting and concentrating capabilities of the LSC. To minimize this photon loss, we have designed a 3D macroporous PC layer that covers both top and bottom surfaces of the QD-based LSC device (Fig. 1a). This PC coating can efficiently recycle the photons otherwise lost through the escape cone, trap and subsequently concentrate them to the edge windows of the LSC device (Fig. 1a).

To demonstrate the enhanced photon trapping effect of the PC coating, we have carried out the Monte Carlo ray-tracing model (MC model) simulation for the LSC devices with and without PC coating [48]. Based on Fresnel Law, we can track the photon propagation of both designs by using a set of vector and location functions. By monitoring a large number of photons, the photon concentrating performances can be evaluated. In order to obtain meaningful comparisons, 30,000 photons (at 365 nm) were set to hit the LSC device normal to the top surface. In the simulation, we considered a cuboid LSC slab with dimensions of 2.8 cm × 1.5 cm × 0.1 cm, and a refractive index (n) of 1.47 (estimated based on the trimethylolpropane ethoxylate triacrylate (TET) and poly (ethylene glycol) diacrylate (PEGDA) copolymer matrix used in the experiments). When 0.2 wt% (with respect to the co-polymer matrix) of QDs was applied to the MC simulation (see simulation details in SI), a drastically increased number of edge-escaped photons (labeled in red arrows) can be directly visualized after PC coating (Fig. 1b and c). Quantitatively, 9.1% of the incident photons can be concentrated to the edge region for the PC-free LSC, whereas, this value increased to 17.6% for the PC-LSC device with the same dimensions and similar amount of the absorbed photons (absorbed ~12800, 42.7% of the total incident photons). Only a slight increase in initially scattered photons (increased by ~360, 1.2% of the total incident photons) after PC coating was simulated, indicating minimal interference between the PC layer and incident photons (outside of the PC stopband), thus the absorption event of the QD emitters inside PC-LSC.

2.2. Band structure and characterizations of CdSe–CdS core-shell QDs

To test the performance of the PC-LSC design in real devices, colloidal CdSe–CdS core-shell QDs with a CdSe core diameter of 3.0 ± 0.2 nm and a CdS shell thickness of 3.8 nm were synthesized following a previously reported method (Fig. 2) [49–51]. The energy diagram for the band structural alignment of the core-shell QD depicts strongly confined hole (localized hole wavefunction inside the core) and weakly confined electron (delocalized electron wavefunction in both core and shell) that are photo-generated in QDs (Fig. 2a) [52,53]. TEM measurements showed that the particles were highly uniform in size and shape with an average diameter of 10.6 ± 0.6 nm (Fig. 2b and S1). High resolution TEM images showed clear cross-fringes of hexagonal atomic lattices, indicating high crystallinity of the sample with a Wurtzite crystal structure, consistent with X-ray powder diffraction

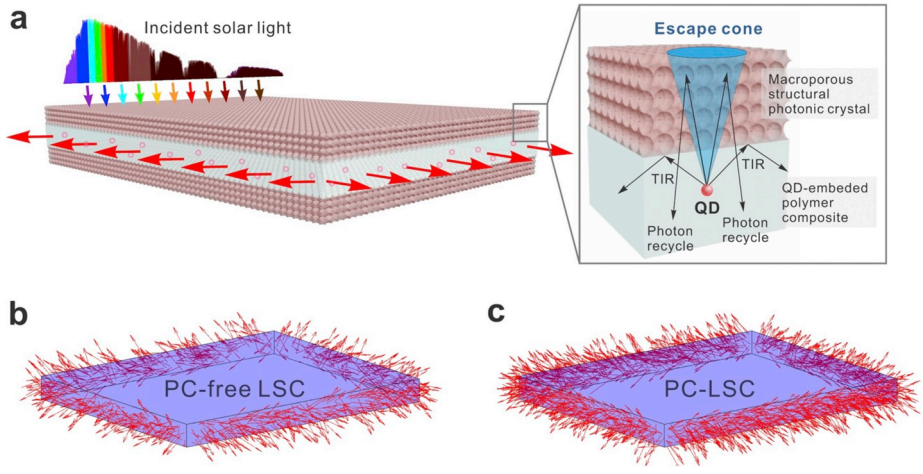

Fig. 1. (a) Schematic representation of the QD-based PC-LSC device (left), and the zoomed-in schematic illustration of the top PC surface and the associated photon trapping mechanism (right). **(b, c)** Visualization of Monte-Carlo ray-tracing simulation for PC-free LSC device (b) and PC-LSC device (c). The red arrows represent the photon output from the edge region of the LSC devices.

measurements (Fig. 2b, inset, and S2). The high morphological uniformity and particle crystallinity of the QDs impart a narrow PL peak centered at 636 nm with a linewidth (full width at half maximum, FWHM) of 85.6 meV (~27.9 nm, Fig. 2c), and a high PL QY of 71% determined by an integrating-sphere. Importantly, due to the presence of a thick CdS shell dominating the absorption event, photon reabsorption processes of the QDs can be largely reduced because of the significantly minimized spectral overlap between the absorption and PL profiles (also referred as 'Stokes-shift-engineered' QDs, Fig. 2c) [19–24, 33,34,54,55]. After incorporating into the TET/PEGDA copolymer slab (QD/polymer, 0.2 wt%), both the absorption and PL spectra remained intact (Fig. 2c), indicating the preservation of QD integrity inside the copolymer matrix and the formation of a QD-polymer solid solution.

2.3. Fabrication and light-trapping performance of PC-LSCs

To fabricate PC-LSC devices, two PC filters consisting of 3D arrays of macropores were coated on the top and bottom surfaces of a QD-embedded LSC copolymer slab (Fig. 3). The fabrication procedure is illustrated in Fig. 3a (see SI for fabrication details). Briefly, a PC filter was first fabricated on a glass substrate by crystallizing colloidal silica spheres through a convective self-assembly process (Fig. 3a) [56–58]. In order to form a double-sided PC coating, a sandwich structure formed from two pieces of PC-coated glass substrates was constructed (Fig. 3a, I), and then filled with a toluene solution of the two mixed monomers (*i.e.,* TET and PEGDA monomers) and the CdSe–CdS QDs (0.2 wt%) (Fig. 3a, II). The entire sandwich structure was photo-polymerized (Fig. 3a, III) at room temperature and then immersed into 2% hydrofluoric acid for 20 s to etch away the silica spheres, resulting in an array of macropores on both sides of the device (Fig. 3a, IV). After triggering with acetone vapor, all the macropores can be fully opened up to form a 3D ordered PC structure with a narrow dielectric photonic stopband (Fig. S3 and Table S1) [57]. It is worth to mention that the PC reflection band may have a blue shift while maintaining the narrow bandwidth when the incident light angle varies from 0° (normal to the surface of PC-LSC) to 90° (parallel to the surface of PC-LSC) [59]. However, given by the wide absorption profile of the QDs (Fig. 2c), we do not expect a significant influence on the overall performance of the PC-LSC device. We also estimated the materials cost for industrial level large-scale production of this PC coating layer to be $0.1575/m^2 (Table S2), representing the low-cost nature of this PC coating method.

One advantage of this PC-LSC system is that the PC stopband position can be easily controlled by tuning the size of macropores [60], allowing for a spectral match with the PL profile of the applied emitters (Fig. S3). This reflection-emission spectral match allows optimal photon trapping efficiency, thus light concentrating performance of the PC-LSC device. In our case, when using the silica spheres with an average diameter of ~400 nm, cross-section scanning electron microscopy (SEM) measurements showed a uniform thickness of the PC layer (~3.0 μm, ~12 monolayers of macropores) with an average pore size of ~375 nm (Fig. 3b and S4). The resulting PC stopband with maximal reflectivity of 96% was centered at ~650 nm with a FWHM of ~220 meV (~87 nm), covering the entire emission spectral region of the embedded QDs in the LSC device (Fig. 4a). The well-defined Fabry-Perot fringes at both sides of the major reflection band demonstrate a high crystallinity of the assembled macroporous structure (Fig. 4a) [53], consistent with the SEM measurements (Fig. 3b and S4). Also, except the reflection and Fabry-Perot fringes region, the PC layer showed a high transparency (~90%) which indicated a low light scattering effect caused by the PC layer (Figure S5). When photons reach the top and bottom surfaces of the LSC within the escape cone (incident angle smaller than the TIR angle), most of them can be recycled by the PC reflector and trapped

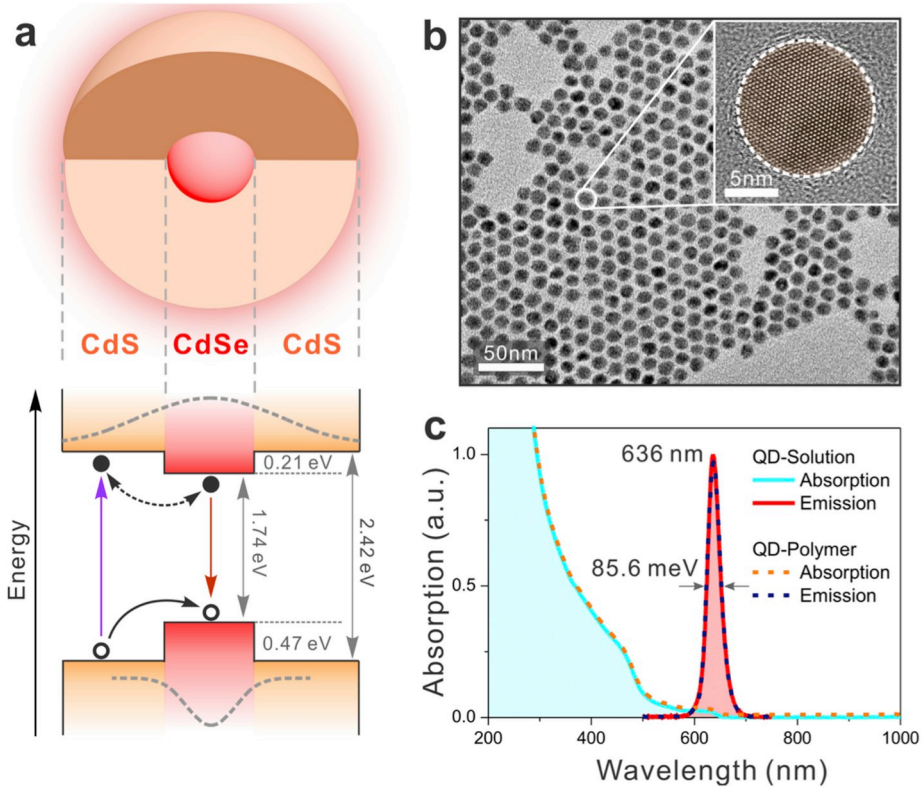

Fig. 2. **(a)** Schematic representation of the CdSe–CdS core-shell QD (top) and the corresponding quasi-Type-II band structural alignment (bottom). **(b)** Typical TEM image of the CdSe–CdS core-shell QDs. Inset: HR-TEM image of one representative core-shell QD. **(c)** Absorption and emission spectra of the CdSe–CdS QDs in hexane solution (solid lines) and in polymer matrix (dashed lines).

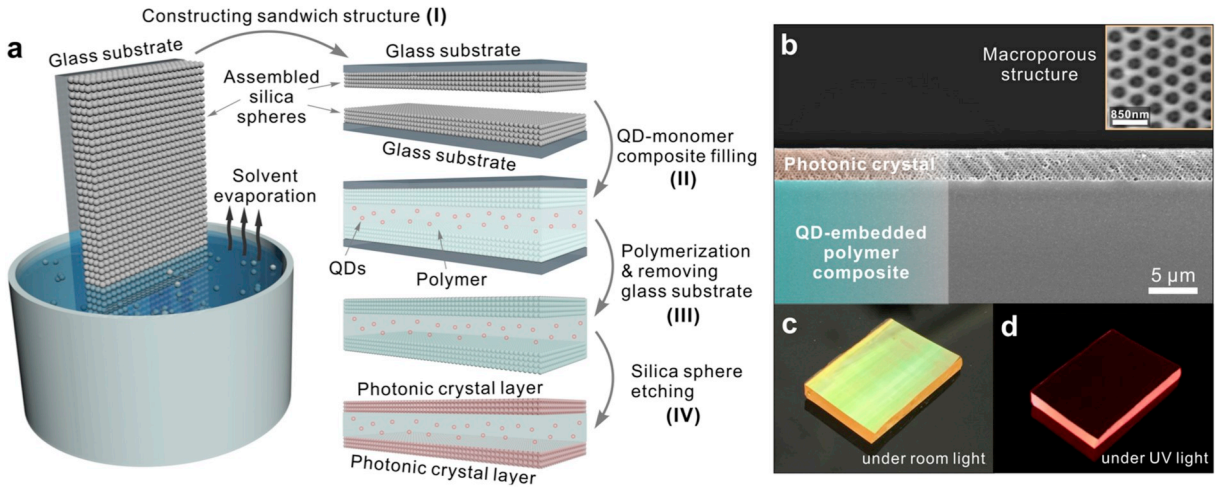

Fig. 3. **(a)** Schematics of fabrication process for macroporous PC coated QD-based LSC copolymer slab. **(b)** Cross-section SEM image of a PC-LSC device. The zoomed-in top-view of the macroporous structure is shown in the right corner. **(c, d)** Photographs of a PC-LSC device (dimensions: 2.8 cm × 1.5 cm × 0.1 cm) illuminated under room light (c) and ultraviolet (UV) light at 365 nm (d).

inside the LSC. The photographs of a PC-LSC device under ambient and 365 nm UV light illumination show a clear light concentrating effect with light dominantly emitted from the edge windows rather than from the top/bottom surfaces of the PC-LSC device (Fig. 3c and d). Quantitative photon-output measurements using an integrating sphere showed that 95.3% of the total collected photons were contributed from the four edges, leaving only 4.7% emitted from the top/bottom surfaces (Fig. 4b), in line with the direct visualization (Fig. 3c and d). As a comparison, only 71.2% of the photons escape from the edges for the conventional PC-free LSC device (Figure S6), indicating a 33.8% enhancement in the photon concentrating effect caused by the PC coating.

2.4. *Simulation and device-performance of PC-LSCs*

To compare the device performances between the conventional PC-free LSC and PC-LSC devices, we have developed an analytical model simulation based on a previously reported method [34,57]. In our

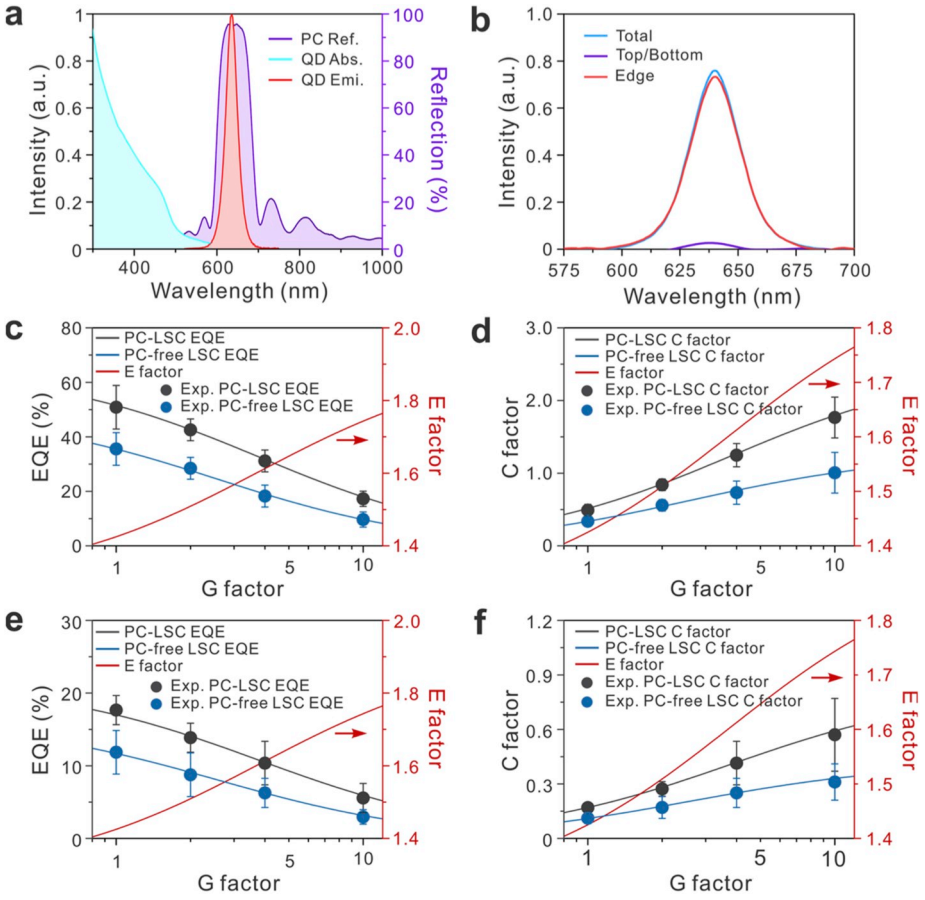

Fig. 4. (a) Reflection (Ref.) spectrum (purple) of the PC reflector as compared with the absorption (Abs., light blue) and emission (Emi., red) spectra of CdSe–CdS core-shell QDs. (b) Emission spectra of total PC-LSC (light blue), edge-covered top/bottom (purple) and the edge emission (red). The dimension of the PC-LSC is 2.8 cm × 1.5 cm × 0.1 cm. (c–f) Simulated EQE (c, e) and C factor (d, f) for PC-free LSC (blue lines) and PC-LSC (black lines) evolutions as a function of G factor under 365 nm single wavelength excitation (c, d) and sunlight illumination (e, f).

model, we considered the solar concentrator waveguide as a square shape LSC slab with four equal edge windows. Without PC coating, the internal quantum efficiency (IQE, η_{int}, defined as the ratio of the edge-collected photon flux and the total absorbed solar flux) and EQE (η_{ext}, defined as the ratio of the edge-collected photon flux and the total incident photon flux) can be expressed as the following equations [61].

$$\eta_{int} = \frac{\eta_{PL}\eta_{trap}}{1+\beta\alpha_2(1-\eta_{PL}\eta_{trap})} \quad (2)$$

$$\eta_{ext} = (1-R)(1-T)\times\eta_{int} = \frac{(1-R)(1-e^{-\alpha_1 d})\eta_{PL}\eta_{trap}}{1+\beta\alpha_2(1-\eta_{PL}\eta_{trap})} \quad (3)$$

Where, η_{PL} is the PL QY of the emitters; η_{trap} is the efficiency of light trapping into the LSC device; R is the reflection coefficient of LSC surfaces; T is the transmission of the overall LSC device; α_1 is the absorption coefficient at the wavelength of incident light; α_2 is reabsorption coefficient at the wavelength of the emitted light; d is the thickness of LSC device, β is a correction factor for elongation of photon light path in a 3D LSC mode versus a 1D mode. In this study, the β value was derived to be 1.8 after MC modelling correction (see SI for details) [36,61].

For the PC-free LSC, η_{trap} is determined solely by TIR, so $\eta_{trap} = \cos\left[\arcsin\left(\frac{1}{n}\right)\right]$. [31,35,61]. However, for the PC-LSC, we need to consider additional reflection processes caused by the top and bottom PC filter coatings. Thus, the $\eta_{trap,\ PC-LSC}$ needs to be modified as:

$$\eta_{trap,\ PC-LSC} = \cos\left[\arcsin\left(\frac{1}{n}\right)\right] + \left\{1-\cos\left[\arcsin\left(\frac{1}{n}\right)\right]\right\} < R > \quad (4)$$

Where, <R> is the reflection factor integrated over the emission profile, which can be expressed as:

$$< R > = \frac{\int S_{PL}(\lambda)R_{PC}(\lambda)d\lambda}{\int S_{PL}(\lambda)d\lambda} \quad (5)$$

The <R> value was calculated to be 0.815 for the PC-LSC device based on experimentally acquired PC reflection and QD emission spectra (Fig. 4a). Therefore, the calculated light trapping efficiency ($\eta_{trap,\ PC-LSC}$) increased from 73.3% for the PC-free LSC to 95.1% for the PC-LSC and agreed well with the experimentally obtained value of 95.3% (Fig. 4b).

Overall, these equations provide accurate descriptions for both IQE (η_{int}) and EQE (η_{ext}). To clearly demonstrate the enhancement effect caused by the PC coating, we further define an enhancement factor (E factor) for the PC-LSC device as compared to PC-free LSC, expressed as:

$$E = \frac{\eta_{ext,\ PC-LSC}}{\eta_{ext,\ LSC}} \quad (6)$$

The simulation results showed that when increasing the geometry gain factor (G, defined as the ratio of the areas of top/bottom surfaces and device edges, G = L/2d, L: square device edge length; d: device thickness) from 1 to 10 while maintaining the device thickness, *i.e.* 1 mm, the η_{ext} for the PC-free LSC and PC-LSC devices decreased from 36.2% to 10.3%, and 51.5% to 17.9%, respectively under 365 nm light illumination (Fig. 4c). These EQE decreases of both PC-free LSC and PC-LSC were mainly attributed to the increased number of reabsorption events, thus the non-radiative decay energy loss of the QDs. Experimental data from measuring the η_{ext} of the fabricated PC-free LSC and PC-LSC devices matched well with the simulation results (Fig. 4c, see SI for details). The E factor calculation, however, showed a continuous increase from 1.43 to 1.74, resulting in a positive correlation in regard to device dimension (Fig. 4c). This E factor increase was also consistent with the improved light trapping efficiency (η_{trap} increased from 73.3% to 95.1%) of the PC-LSC, in line with the MC simulation (Fig. 1). Taking both EQE and G factor into consideration for the overall photon concentrating performances, we calculated the C factor (defined as the ratio of the output and the input photon flux densities, $C = \eta_{ext} \times G$) evolution as a function of G factor. As shown in Fig. 4d, a continuous increase of C factor from 0.52 (0.36) to 1.79 (1.03) was obtained for the PC-LSC (PC-free LSC) upon increasing the G value from 1 to 10. Fig. 4e and f shows the simulated evolutions of η_{ext}, C factor, and their associated E factor under sunlight (1.5 a.m. Global) illumination, all of which show similar trends as those under 365 nm light illumination (Fig. 4c and d). To validate these theoretical modelling and simulated results, we have performed optoelectronic studies by integrating silicon-based PVs to the edge of our LSCs. The η_{ext} and C factor were then measured through measuring the *I–V* curve of the integrated LSC-PV devices under simulated solar light irradiation (see SI for details). Excellent consistencies between the experimentally obtained η_{ext} and C factors and our theoretically simulated results were obtained (Fig. 4e and f). An E factor of ~1.8 for both EQE and C factor (at G = 10) was obtained in the LSC-PV systems, and agreed well with the simulated value of 1.74. Our results demonstrated a reliable enhancement of device performance by the PC coating for the LSCs for all geometry designs under real device working conditions.

2.5. Simulation study of G-factor and enhancement factor of PC-LSCs

In previous studies, G factor has been generally considered as the major geometrical parameter that may affect the LSC quantum efficiencies (both η_{int} and η_{ext}) [34,36,54,61,62]. However, during the simulation study, we found that by altering the total volume of the LSC device while maintaining the same G factor (*i.e.,* simultaneously scaling three dimensions of the LSC), the η_{ext} of the device could be significantly altered. The instability of the η_{ext} for the LSC with different total volumes but constant G factors can be attributed to the absorption/reabsorption events of the emitters during light propagation inside the LSCs. In other words, a larger device (with a large thickness, d, of the LSC) allows increased absorption of incident photons by embedded emitters before reaching device absorption saturation. In this case, more emitted photons will be concentrated by the LSC, and contribute to an enhancement of the η_{ext} of the device. On the other hand, in a larger device, the emitted photons need to travel a longer propagation path than that for a smaller device before reaching edge windows. As a result, the photons will have a higher probability of being reabsorbed by another emitter (*i.e.,* QD), and then lost through *e.g.* non-radiative events (due to sub-unity PL QY), thus contributing to a decrease the η_{ext} of the LSC. When considering these two competing effects, the existence of an optimal device volume (*i.e.* device thickness) with the highest η_{ext} value for an LSC device of fixed G factor should be anticipated. By applying our simulation model, we mapped out the optimal device thickness (d) for LSCs with varying G factors under either 365 nm light or sunlight (1.5 a.m. Global) illumination (Fig. 5a–f, S7 and S8). Note that, in these simulations, we decreased the QD concentration to 0.1 wt% in order to achieve a wider simulation range for the device thickness before saturating the light absorption. The simulation result confirmed the existence of an optimal device thickness (device volume) with the highest η_{ext} for PC-free LSC and PC-LSC devices. Moreover, different optimal device thickness (d) and EQE (η_{ext}) were also observed for different given G factors (Fig. 5a–c and S7). For example, when G = 20 and under 365 nm light excitation, an optimal d of 14 mm was calculated with the highest η_{ext} of 25.8% for a conventional PC-free LSC. These values shifted to 16 mm and 38.3% for the corresponding PC-LSC (Fig. 5b). Similarly, we have also investigated the C factor behavior under 365 nm light and sunlight illuminations. When the G factor was kept constant at 100, the C factor for the PC-free LSC device was calculated to be 3.97 at an optimal thickness of 12 mm (Fig. 5f). However, for the PC-LSC device, the optimal device thickness shifted to 14 mm and the C factor showed a 59.2% enhancement reaching to a maximal value of 6.32 (Fig. 5f). Our simulation results reveal that, in order to achieve the best light concentrating performance, specific geometric design and optimization processes of the LSC device need to be carried out before integration into

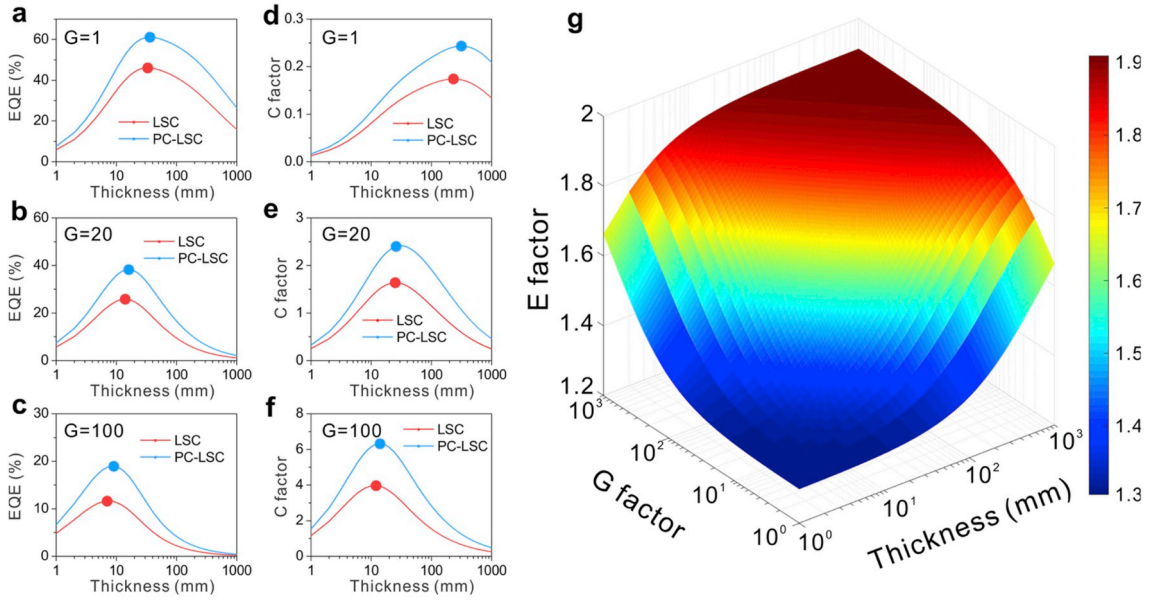

Fig. 5. **(a–c)** External quantum efficiency (EQE) of the PC-free LSC (red line) and PC-LSC (blue line) as a function of device thickness under 365 nm light excitation at G factor values of 1 (a,), 20 (b) and 100 (c). **(d–f)** Concentration factor (C factor) of the LSC (red line) and PC-LSC (blue line) as a function of device thickness under sunlight (1.5 a.m. Global) illumination at G factor values of 1 (d), 20 (e) and 100 (f). The blue and red dots in (a–f) indicate the maximal point of the EQE (a–c) and C factor (d–f). **(g)** 3D plot of the enhancement factor (E factor) evolution under sunlight (1.5 a.m. Global) illumination as functions of G factor and device thickness. The QD emitter concentration is set as 0.1 wt% in all simulations.

a solar energy harvesting system.

Our simulation results unambiguously confirmed the enhancement of device performance caused by applying a PC reflector to conventional LSCs (Figs. 4 and 5). For clear visualization of this enhancement effect, we constructed 3D plot of the enhancement factor (E) as functions of G factor and device thickness (d) under sunlight (1.5 a.m. Global) illumination (Fig. 5g). Upon increasing both the G factor and d, the E factor continuously increased and plateaued at ~1.9 as the G factor and thickness reached large values of *e.g.* ~1000 and ~1000 mm, respectively. Nearly the same device enhancement effects can be gained under 365 nm light illumination (Fig. S9), indicating stable enhancement of device performance independent of the types of incident light. Moreover, we noticed that the E factor is highly sensitive to the quality of the emitters and the PC reflector. This can be attributed to a negative (positive) correlation between the escape photon loss and the <R> value (G factor) of the PC-LSC with a defined device thickness (Fig. S10). When a unity value for the PL QY of the emitter and 0.9 for the <R> of the PC reflector coating were applied in our simulation model, the E factor was significantly boosted up to 11.5 (at $G = 1000$, $d = 1$ mm), indicating more than an order of magnitude enhancements for both EQE and C factor of the LSC devices (Fig. S11). The E factor could be further elevated above 13 upon further geometrical optimizations (*e.g.*, increasing the device thickness, Fig. S12).

3. Conclusions and perspectives

We demonstrate a 3D macroporous PC filter coating on QD-based LSC devices with enhanced light concentrating performance through both experimental studies and computer simulations. We show that the narrow PC reflection band can be tuned to perfectly cover the emission profile of the applied QDs in the LSCs. Compared with the conventional PC-free LSC devices, the PC-LSC shows significant enhancements for both EQE and C factor at different G factors. According to the simulation study, we demonstrate a basic principle for LSC and PC-LSC geometrical design. Furthermore, the tunable reflection window of the 3D macroporous PC with narrow reflection band offers the possibility for creating tandem LSCs consisting of multi-type emitters with optimized reflection-emission matched PC coatings. Our study sheds light on the future design and fabrication of the LSCs with optimal light concentrating capabilities well-beyond conventional escape cone-limited LSCs.

Author contributions

J. W. and O. C. conceived the idea. Y. Y. and H. Z. carried out the QDs synthesis and characterizations. J. W. conducted out the PC-LSC fabrication and characterization. J. W. performed out the SEM measurement. H. Z. and Y. Y. carried out the TEM measurement. J. W. and T. C. conducted the XRD measurement. J. W. and Y. Y. performed the PL QY measurement. J. W. carried out the MC simulations and analytical mode simulations. J. W., H. Z. and Y. Y. analyzed the data. J. W. and O. C. wrote the manuscript. All the authors commented on the manuscript. O. C. supervised the entire project.

Declaration of competing interest

The authors declare no competing interests.

Acknowledgements

O. C. acknowledges support from Brown University startup funds, the IMNI seed fund and the National Science Foundation (CBET-1936223). SEM, TEM and XRD measurements were performed at the Electron Microscopy Facility in the Institute for Molecular and Nanoscale Innovation (IMNI) at Brown University. J. W. thanks Zhenghong Dai for optoelectronic devices measurements.

Appendix A. Supplementary data

Supplementary data to this article can be found online at https://doi.org/10.1016/j.nanoen.2019.104217.

References

[1] P. Erickson, M. Lazarus, G. Piggot, Limiting fossil fuel production as the next big step in climate policy, Nat. Clim. Change 8 (12) (2018) 1037–1043.

[2] T. Van de Graaf, J. Colgan, Global energy governance: a review and research agenda, Palgrave Commun. 2 (1) (2016) 1–12.
[3] J. Zheng, S. Suh, Strategies to reduce the global carbon footprint of plastics, Nat. Clim. Change 9 (5) (2019) 374–378.
[4] S. Sgouridis, M. Carbajales-Dale, D. Csala, M. Chiesa, U. Bardi, Comparative net energy analysis of renewable electricity and carbon capture and storage, Nat. Energy 4 (6) (2019) 456–465.
[5] P. Cheng, G. Li, X. Zhan, Y. Yang, Next-generation organic photovoltaics based on non-fullerene acceptors, Nat. Photonics 12 (3) (2018) 131–142.
[6] S. Chu, A. Majumdar, Opportunities and challenges for a sustainable energy future, Nature 488 (7411) (2012) 294–303.
[7] R. Gross, R. Hanna, Path dependency in provision of domestic heating, Nat. Energy 4 (2019) 358–364.
[8] C. Fei Guo, T. Sun, F. Cao, Q. Liu, Z. Ren, Metallic nanostructures for light trapping in energy-harvesting devices, Light Sci. Appl. 3 (4) (2014) e161.
[9] M. Kumar, S. Kumar, Liquid crystals in photovoltaics: a new generation of organic photovoltaics, Polym. J. 49 (1) (2016) 85–111.
[10] X. Guo, P. Yi, Y. Yang, J. Cui, S. Xiao, W. Wang, Effects of surfactants on agarose-based magnetic polymer electrolyte for dye-sensitized solar cells, Electrochim. Acta 90 (2013) 524–529.
[11] F. Niehaus, J. Williams, Studies of different energy strategies in terms of their effects on the atmospheric CO2concentration, J. Geophys. Res. 84 (C6) (1979) 3123–3129.
[12] K. Zhu, N.R. Neale, A. Miedaner, A.J. Frank, Enhanced charge-collection efficiencies and light scattering in dye-sensitized solar cells using oriented TiO2 nanotubes arrays, Nano Lett. 7 (1) (2007) 69–74.
[13] J.S. Batchelder, A.H. Zewail, T. Cole, Luminescent solar concentrators. 1: theory of operation and techniques for performance evaluation, Appl. Opt. 18 (18) (1979) 3090–3110.
[14] W.G. van Sark, K.W. Barnham, L.H. Slooff, A.J. Chatten, A. Buchtemann, A. Meyer, S.J. McCormack, R. Koole, D.J. Farrell, R. Bose, E.E. Bende, A.R. Burgers, T. Budel, J. Quilitz, M. Kennedy, T. Meyer, M. Donega Cde, A. Meijerink, D. Vanmaekelbergh, Luminescent Solar Concentrators–e, Opt. Express 16 (26) (2008) 21773–21792.
[15] F. Meinardi, F. Bruni, S. Brovelli, Luminescent solar concentrators for building-integrated photovoltaics, Nat. Rev. Mater. 2 (12) (2017) 17072.
[16] M. Debije, P. Verbunt, Thirty years of luminescent solar concentrator research: solar energy for the built environment, Adv. Energy Mater. 2 (1) (2012) 12–35.
[17] R. Evans, B. Mckenna, Towards efficient spectral converters through materials design for luminescent solar devices, Adv. Mater. 29 (28) (2017) 1606491.
[18] W.H. Weber, J. Lambe, Luminescent greenhouse collector for solar radiation, Appl. Opt. 15 (10) (1976) 2299–2300.
[19] F. Meinardi, A. Colombo, K.A. Velizhanin, R. Simonutti, M. Lorenzon, L. Beverina, R. Viswanatha, V.I. Klimov, S. Brovelli, Large-area luminescent solar concentrators based on 'Stokes-shift-engineered' nanocrystals in a mass-polymerized PMMA matrix, Nat. Photonics 8 (5) (2014) 392–399.
[20] X. Luo, T. Ding, X. Liu, Y. Liu, K. Wu, Quantum cutting luminescent solar concentrators using ytterbium doped perovskite nanocrystals, Nano Lett. 19 (1) (2018), 338-34.
[21] I. Coropceanu, M.G. Bawendi, Core/shell quantum dot based luminescent solar concentrators with reduced reabsorption and enhanced efficiency, Nano Lett. 14 (7) (2014) 4097–4101.
[22] C. Li, W. Chen, D. Wu, D. Quan, Z. Zhou, J. Hao, J. Qin, Y. Li, Z. He, K. Wang, Large Stokes shift and high efficiency luminescent solar concentrator incorporated with CuInS2/ZnS quantum dots, Sci. Rep. 5 (2015) 17777.
[23] K.E. Knowles, T.B. Kilburn, D.G. Alzate, S. McDowall, D.R. Gamelin, Bright CuInS2/CdS nanocrystal phosphors for high-gain full-spectrum luminescent solar concentrators, Chem. Commun. 51 (44) (2015) 9129–9132.
[24] F. Meinardi, H. McDaniel, F. Carulli, A. Colombo, K.A. Velizhanin, N.S. Makarov, R. Simonutti, V.I. Klimov, S. Brovelli, Highly efficient large-area colourless luminescent solar concentrators using heavy-metal-free colloidal quantum dots, Nat. Nanotechnol. 10 (10) (2015) 878–885.
[25] K. Sun, M. Vasudev, H.-S. Jung, J. Yang, A. Kar, Y. Li, K. Reinhardt, P. Snee, M. A. Stroscio, M. Dutta, Applications of colloidal quantum dots, Microelectron. J. 40 (3) (2009) 644–649.
[26] L.R. Bradshaw, K.E. Knowles, S. McDowall, D.R. Gamelin, Nanocrystals for luminescent solar concentrators, Nano Lett. 15 (2) (2015) 1315–1323.
[27] Y. Zhou, D. Benetti, X. Tong, L. Jin, Z.M. Wang, D. Ma, H. Zhao, F. Rosei, Colloidal carbon dots based highly stable luminescent solar concentrators, Nano Energy 44 (2018) 378–387.
[28] G. Liu, R. Mazzaro, Y. Wang, H. Zhao, A. Vomiero, High efficiency sandwich structure luminescent solar concentrators based on colloidal quantum dots, Nano Energy 60 (2019) 119–126.
[29] H. Zhao, Y. Zhou, D. Benetti, D. Ma, F. Rosei, Perovskite quantum dots integrated in large-area luminescent solar concentrators, Nano Energy 37 (2017) 214–223.
[30] S. McDowall, T. Butler, E. Bain, K. Scharnhorst, D. Patrick, Comprehensive analysis of escape-cone losses from luminescent waveguides, Appl. Opt. 52 (6) (2013) 1230–1239.
[31] M. Debije, P. Verbunt, B. Rowan, B. Richards, J. Hoeks, Measured surface loss from luminescent solar concentrator waveguides, Appl. Opt. 47 (36) (2008) 6763–6768.
[32] L. Xu, Y. Yao, N.D. Bronstein, L. Li, A.P. Alivisatos, R.G. Nuzzo, Enhanced photon collection in luminescent solar concentrators with distributed Bragg reflectors, ACS Photonics 3 (2) (2016) 278–285.
[33] N.D. Bronstein, Y. Yao, L. Xu, E. O'Brien, A.S. Powers, V.E. Ferry, A.P. Alivisatos, R. G. Nuzzo, Quantum dot luminescent concentrator cavity exhibiting 30-fold concentration, ACS Photonics 2 (11) (2015) 1576–1583.
[34] M. Sharma, K. Gungor, A. Yeltik, M. Olutas, B. Guzelturk, Y. Kelestemur, T. Erdem, S. Delikanli, J.R. McBride, H.V. Demir, Near-unity emitting copper-doped colloidal semiconductor quantum wells for luminescent solar concentrators, Adv. Mater. 29 (30) (2017) 1700821.
[35] C.S. Erickson, L.R. Bradshaw, S. McDowall, J.D. Gilbertson, D.R. Gamelin, D. L. Patrick, Zero-reabsorption doped-nanocrystal luminescent solar concentrators, ACS Nano 8 (4) (2014) 3461–3467.
[36] H.J. Song, B.G. Jeong, J. Lim, D.C. Lee, W.K. Bae, V.I. Klimov, Performance limits of luminescent solar concentrators tested with seed/quantum-well quantum dots in a selective-reflector-based optical cavity, Nano Lett. 18 (1) (2018) 395–404.
[37] S.M. Jeong, K. Sonoyama, Y. Takanishi, K. Ishikawa, H. Takezoe, S. Nishimura, G. Suzaki, M.H. Song, Optical cavity with a double-layered cholesteric liquid crystal mirror and its prospective application to solid state laser, Appl. Phys. Lett. 89 (24) (2006) 241116.
[38] M.G. Debije, M.P. Van, P.P. Verbunt, M.J. Kastelijn, R.H. van der Blom, D.J. Broer, C.W. Bastiaansen, Effect on the output of a luminescent solar concentrator on application of organic wavelength-selective mirrors, Appl. Opt. 49 (4) (2010) 745–751.
[39] D. Boer, D. Broer, M. Debije, W. Keur, A. Meijerink, C. Ronda, P. Verbunt, Progress in phosphors and filters for luminescent solar concentrators, Opt. Express 20 (S3) (2012) A395–A405.
[40] M. Peters, J.C. Goldschmidt, P. Löper, B. Bläsi, A. Gombert, The effect of photonic structures on the light guiding efficiency of fluorescent concentrators, J. Appl. Phys. 105 (1) (2009) 014909.
[41] H.M. Ng, T.D. Moustakas, S.N.G. Chu, High reflectivity and broad bandwidth AlN/GaN distributed Bragg reflectors grown by molecular-beam epitaxy, Appl. Phys. Lett. 76 (20) (2000) 2818–2820.
[42] A.J. Nolte, M.F. Rubner, R.E. Cohen, Creating effective refractive index gradients within polyelectrolyte multilayer films: molecularly assembled rugate filters, Langmuir 20 (8) (2004) 3304–3310.
[43] C.C. Lee, C.J. Tang, J.Y. Wu, Rugate filter made with composite thin films by ion-beam sputtering, Appl. Opt. 45 (7) (2006) 1333–1337.
[44] C. Pina-Hernandez, A. Koshelev, S. Dhuey, S. Sassolini, M. Sainato, S. Cabrini, K. Munechika, Nanoimprinted high-refractive index active photonic nanostructures based on quantum dots for visible light, Sci. Rep. 7 (1) (2017) 17645.
[45] E. Lorenzo, C.J. Oton, N.E. Capuj, M. Ghulinyan, D. Navarro-Urrios, Z. Gaburro, L. Pavesi, Porous silicon-based rugate filters, Appl. Opt. 44 (26) (2005) 5415–5421.
[46] H.A. Abusafia, A.I. Alsharif, I.O. Abualjarayesh, Rugate filter sidelobe suppression using half-apodization, Appl. Opt. 32 (25) (1993) 4831–4835.
[47] K. Aoki, G. Guimard, M. Nishioka, M. Nomura, S. Iwamoto, Y. Arakawa, Coupling of quantum-dot light emission with a three-dimensional photonic-crystal nanocavity, Nat. Photonics 2 (2008) 688–692.
[48] X. Hu, R. Kang, Y. Zhang, L. Deng, H. Zhong, B. Zou, L.J. Shi, Ray-trace simulation of CuInS(Se)(2) quantum dot based luminescent solar concentrators, Opt. Express 23 (15) (2015) A858–A867.
[49] O. Chen, J. Zhao, V.P. Chauhan, J. Cui, C. Wong, D.K. Harris, H. Wei, H.S. Han, D. Fukumura, R.K. Jain, M.G. Bawendi, Compact high-quality CdSe-CdS core-shell nanocrystals with narrow emission linewidths and suppressed blinking, Nat. Mater. 12 (5) (2013) 445–451.
[50] R. Tan, Y. Yuan, Y. Nagaoka, D. Eggert, X. Wang, S. Thota, P. Guo, H. Yang, J. Zhao, O. Chen, Monodisperse hexagonal pyramidal and bipyramidal wurtzite CdSe-CdS core–shell nanocrystals, Chem. Mater. 29 (9) (2017) 4097–4108.
[51] B. Li, K. Bian, X. Zhou, P. Lu, S. Liu, I. Brener, M. Sinclair, T. Luk, H. Schunk, L. Alarid, P.G. Clem, Z. Wang, H. Fan, Pressure compression of CdSe nanoparticles into luminescent nanowires, Sci. Adv. 3 (5) (2017), e1602916.
[52] P. Reiss, M. Protiere, L. Li, Core/Shell semiconductor nanocrystals, Small 5 (2) (2009) 154–168.
[53] N. McElroy, R.C. Page, D. Espinbarro-Valazquez, E. Lewis, S. Haigh, P. O'Brien, D. J. Binks, Comparison of solar cells sensitised by CdTe/CdSe and CdSe/CdTe core/shell colloidal quantum dots with and without a CdS outer layer, Thin Solid Films 560 (2014) 65–70.
[54] H. Li, K. Wu, J. Lim, H.-J. Song, V.I. Klimov, Doctor-blade deposition of quantum dots onto standard window glass for low-loss large-area luminescent solar concentrators, Nat. Energy 1 (12) (2016) 16157.
[55] K. Wu, H. Li, V.I. Klimov, Tandem luminescent solar concentrators based on engineered quantum dots, Nat. Photonics 12 (2) (2018) 105–110.
[56] P. Jiang, J.F. Bertone, K.S. Hwang, V.L. Colvin, Single-crystal colloidal multilayers of controlled thickness, Chem. Mater. 11 (8) (1999) 2132–2140.
[57] Y. Fang, Y. Ni, B. Choi, S.Y. Leo, J. Gao, B. Ge, C. Taylor, V. Basile, P. Jiang, Chromogenic photonic crystals enabled by novel vapor-responsive shape-memory polymers, Adv. Mater. 27 (24) (2015) 3696–3704.
[58] Y. Ni, Y. Zhang, S.-Y. Leo, Y. Fang, M. Zhao, L. Yu, K.D. Schulze, W.G. Sawyer, T. E. Angelini, P. Jiang, C.R. Taylor, Unconventional shape memory mechanisms of nanoporous polymer photonic crystals: implications for nano-optical coatings and devices, ACS Appl. Nano Mater. 1 (11) (2018) 6081–6090.
[59] E. Gaulding, G. Liu, C. Chen, L. Lobbert, A. Li, G. Segev, J. Eichhorn, S. Aloni, A. Schwatzberg, I. Sharp, F. Toma, Fabrication and optical characterization of polystyrene opal templates for the synthesis of scalable, nanoporous (photo) electrocatalytic materials by electrodeposition, J. Mater. Chem. A 5 (2017) 11601–11614.
[60] P. Jiang, M. McFarland, J. Am. Chem. Soc. 126 (42) (2004) 13778–13786.
[61] V.I. Klimov, T.A. Baker, J. Lim, K.A. Velizhanin, H. McDaniel, Quality factor of luminescent solar concentrators and practical concentration limits attainable with semiconductor quantum dots, ACS Photonics 3 (6) (2016) 1138–1148.
[62] H. Zhao, D. Benetti, X. Tong, H. Zhang, Y. Zhou, G. Liu, D. Ma, S. Sun, Z.M. Wang, Y. Wang, F. Rosei, Efficient and stable tandem luminescent solar concentrators

based on carbon dots and perovskite quantum dots, Nano Energy 50 (2018) 756–765.

Junyu Wang is currently a Ph.D. candidate in Prof. Ou Chen's group at Brown University. He received his M.S. degree in Material Science Engineering from University of Florida in 2017 and B.S. degree in Chemistry from Southeast University, Nanjing, China. His research interests include the fabrication and simulation of quantum dots based luminescent solar concentrators,self-assembled photonic crystal and nanomaterial device development, etc.

Yucheng Yuan obtained her B.S. degree in pharmaceutical sciences in 2012 and M.S. degree in pharmaceutical chemistry in 2015 at Tianjin University, Tianjin, China. She is now a Ph.D. candidate in Prof. Ou Chen's group at Brown University. Her research interests include the development of new synthetic methodologies to produce semiconductor nanocrystals with desired properties and the applications in solar energy harvesting, biological imaging, and photocatalysis, etc.

Hua Zhu obtained his B.S. degree in chemistry in 2015 at Fudan University, Shanghai, China. He is now a Ph.D. candidate in Prof. Ou Chen's group in Brown University. His research interests include the synthesis and self-assembly of multicomponent heterostructual nanocrystals as well as their properties far from the thermal equilibrium.

Tong Cai is currently a Ph.D. candidate in the Department of Chemistry at Brown University. He received his B.S. degree in Chemistry and B.A. degree in Economics from Peking University in 2017. His research concentrates on synthesizing multifunctional nanomaterials and exploring their novel properties with potential applications.

Yin Fang received his Ph.D. in chemical engineering from the University of Florida in 2016. His Ph.D. research focused on the self-assembled photonic crystals, shape memory polymers, smart windows and the plasmonic sensing in photonic structures. He accolades during his Ph.D. include MRS graduate student award (2015), Chinese government award for outstanding self-financed Ph.D. students (2016).

Ou Chen is an assistant professor in the Department of Chemistry at the Brown University. He received his B.S. degree in Chemical Physics from the University of Science and Technology of China (USTC) in 2004, and completed his PhD study in the Department of Chemistry at the University of Florida. After postdoctoral training working with Prof. Moungi Bawendi at MIT, he joined the Brown University in fall 2015. Prof. Ou Chen's current research interests focus on exploring novel methodologies for fabrications of functional nanocrystals, semiconductor quantum dots, perovskite nanomaterials and their self-assembled higher-order superstructures for energy, catalysis and bio-related applications.